

Supporting Information for

Structural and Optical Control through Anion and Cation  
Exchange Processes for Sn-Halide Perovskite Nanostructures

*Kushagra Gahlot,<sup>1</sup> Julius Meijer<sup>1</sup> and Loredana Protesescu<sup>1,\*</sup>*

Zernike Institute for Advanced Materials, University of Groningen, Nijenborgh 4, Groningen,  
9747AG, The Netherlands.

Corresponding author: Dr. Loredana Protesescu, E-mail: [l.protesescu@rug.nl](mailto:l.protesescu@rug.nl)

## Contents

	Description	Page
<b>Figure S1</b>	Powder X-ray diffraction pattern of 2D RP structures quenched with and without ice-water.	3
<b>Figure S2</b>	Powder X-ray diffraction pattern and UV-Visible spectroscopy before and after cation exchange in 2D [R-NH <sub>3</sub> ] <sub>2</sub> SnBr <sub>4</sub> RP perovskite nanostructures.	4
<b>Figure S3</b>	SEM images (transmission mode at 18 kV) of FASnI <sub>3</sub> NCs formed via cation exchange of 2D [R-NH <sub>3</sub> ] <sub>2</sub> SnI <sub>4</sub> RP nanostructures.	5
<b>Figure S4</b>	Extended time-dependent UV-Visible spectroscopy measurements of the cation exchange reaction.	6
<b>Figure S5</b>	Concentration dependent UV-Visible spectroscopy measurements of cation exchange in 2D [R-NH <sub>3</sub> ] <sub>2</sub> SnBr <sub>4</sub> RP perovskite nanostructures.	7
<b>Figure S6</b>	SEM images (transmission mode at 18 kV) of 2D [R-NH <sub>3</sub> ] <sub>2</sub> SnX <sub>4</sub> RP perovskite nanostructures in lens detector mode.	8
<b>Figure S7</b>	Cation Exchange in thin-films - Annealing temperature dependence in Sn-halide perovskite thin-films with A cation addition at different concentrations.	9
<b>Figure S8</b>	X-ray diffraction pattern of degraded thin-film after excess Cs(OI) addition for cation exchange.	10
<b>Figure S9</b>	UV-Visible and PL spectroscopy of anion exchange on CsSnI <sub>3</sub> NCs.	10
<b>Figure S10</b>	Anion exchange process via SEM Micrographs from CsSnI <sub>3</sub> NCs to CsSnBr <sub>3</sub> NCs and CsSnBr <sub>3</sub> NCs to CsSnCl <sub>3</sub> NCs.	11
<b>Figure S11</b>	Powder X-ray diffraction pattern, UV-Visible and PL spectroscopy of anion exchange on CsSnBr <sub>3</sub> NCs.	11
<b>Figure S12</b>	X-ray diffraction pattern evolution with different amount of BzI added for anion exchange	12

## Supporting Figures

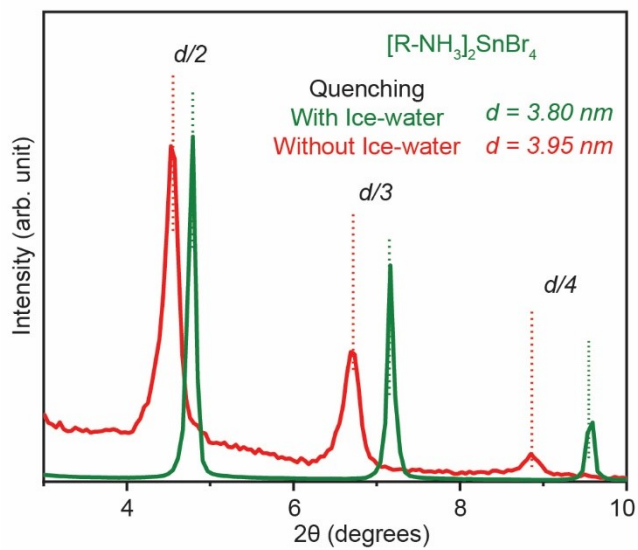


Figure S1. Powder X-ray diffraction pattern of the 2D  $[R-NH_3]_2SnBr_4$   $n = 1$  RP nanostructures with reaction quenched with ice-water (green) and without ice-water (red).

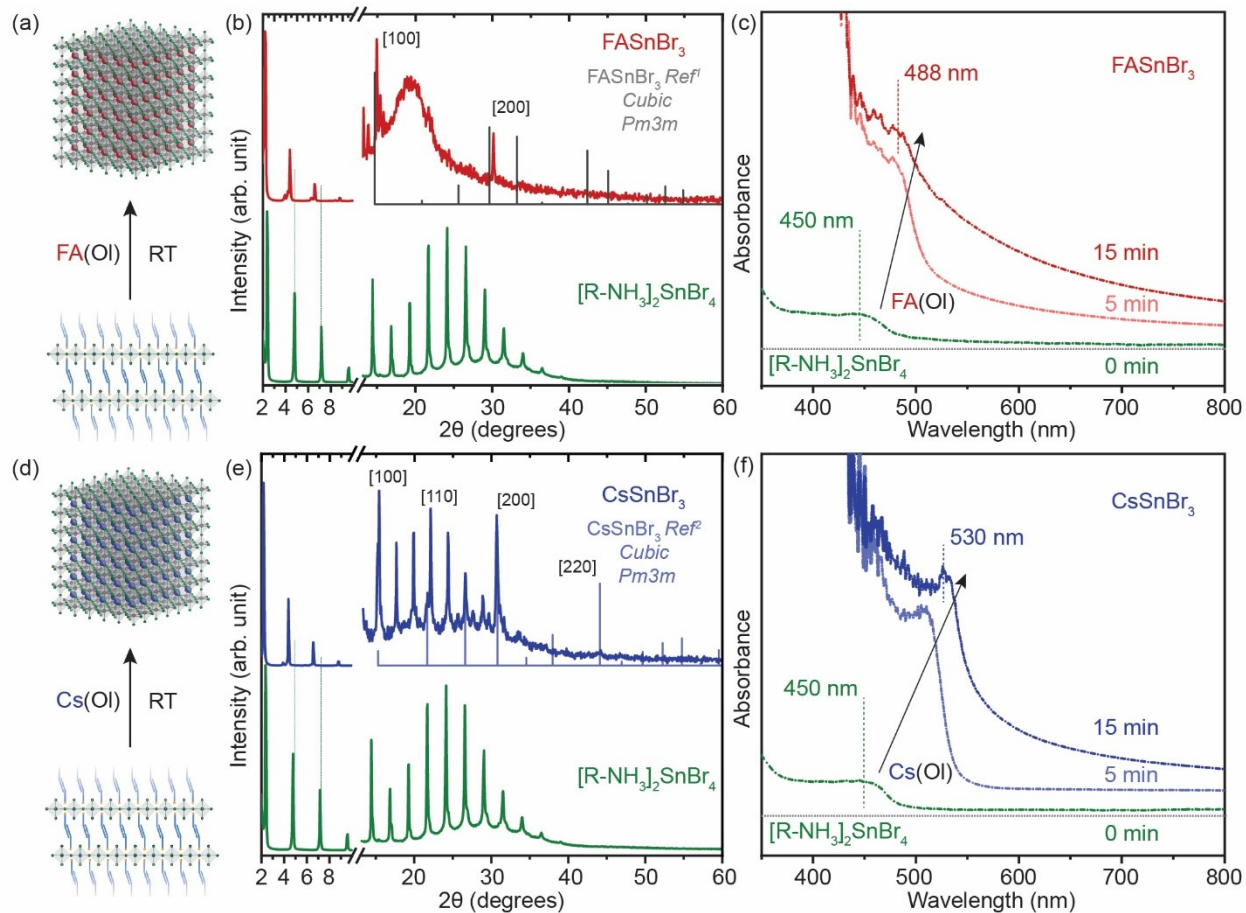
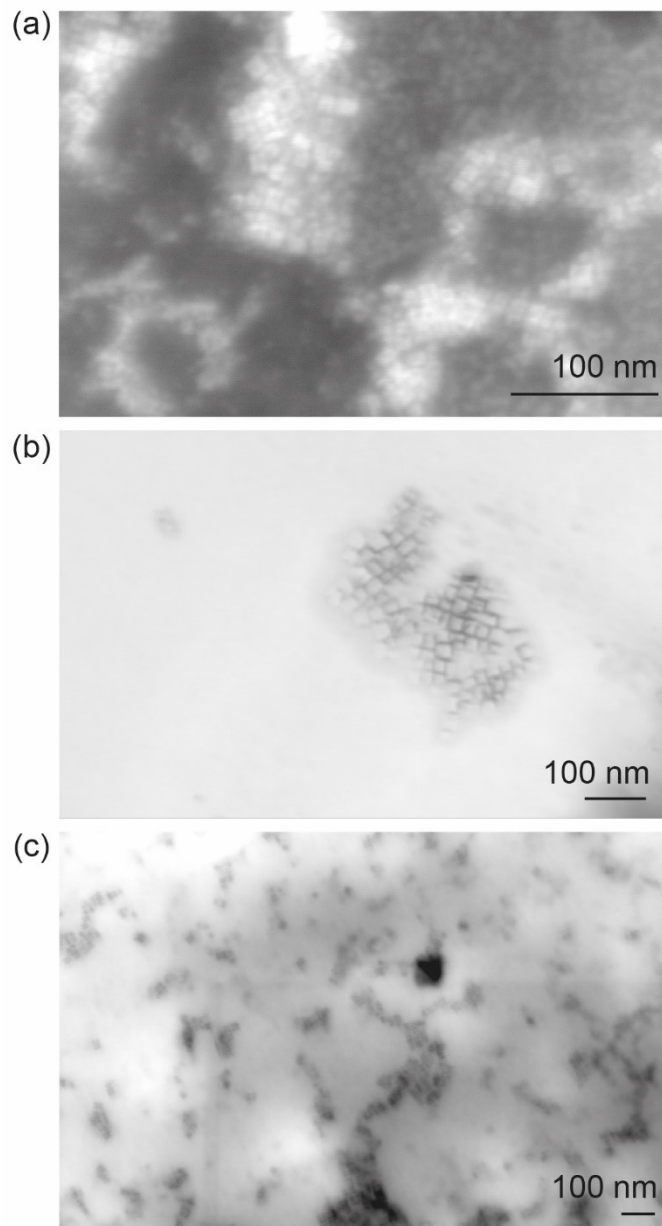


Figure S2. (a) and (d) Schematic representation of conversion of 2D  $[R-NH_3]_2SnBr_4$  to 3D  $FASnBr_3$  and  $CsSnBr_3$  NCs respectively. (b) and (e) Powder X-ray diffraction pattern of the converted 3D  $FASnBr_3$  (red) and  $CsSnBr_3$  (blue) NCs from 2D  $[R-NH_3]_2SnBr_4$  respectively. (c) and (f) In-situ UV-Visible spectroscopy of the formation of 3D  $FASnBr_3$  (red) and  $CsSnBr_3$  (blue) NCs from 2D  $[R-NH_3]_2SnBr_4$  RP structure with the addition of A cation. The XRD references were adapted from ref.<sup>1</sup> for  $FASnBr_3$  (cubic,  $Pm3m$ ) and ref.<sup>2</sup> for  $CsSnBr_3$  (cubic,  $Pm3m$ ).



*Figure S3. SEM images of  $FASnI_3$  NCs formed via cation exchange of  $2D [R-NH_3]_2SnI_4$  RP nanostructures at decreasing magnifications from (a) to (c).*

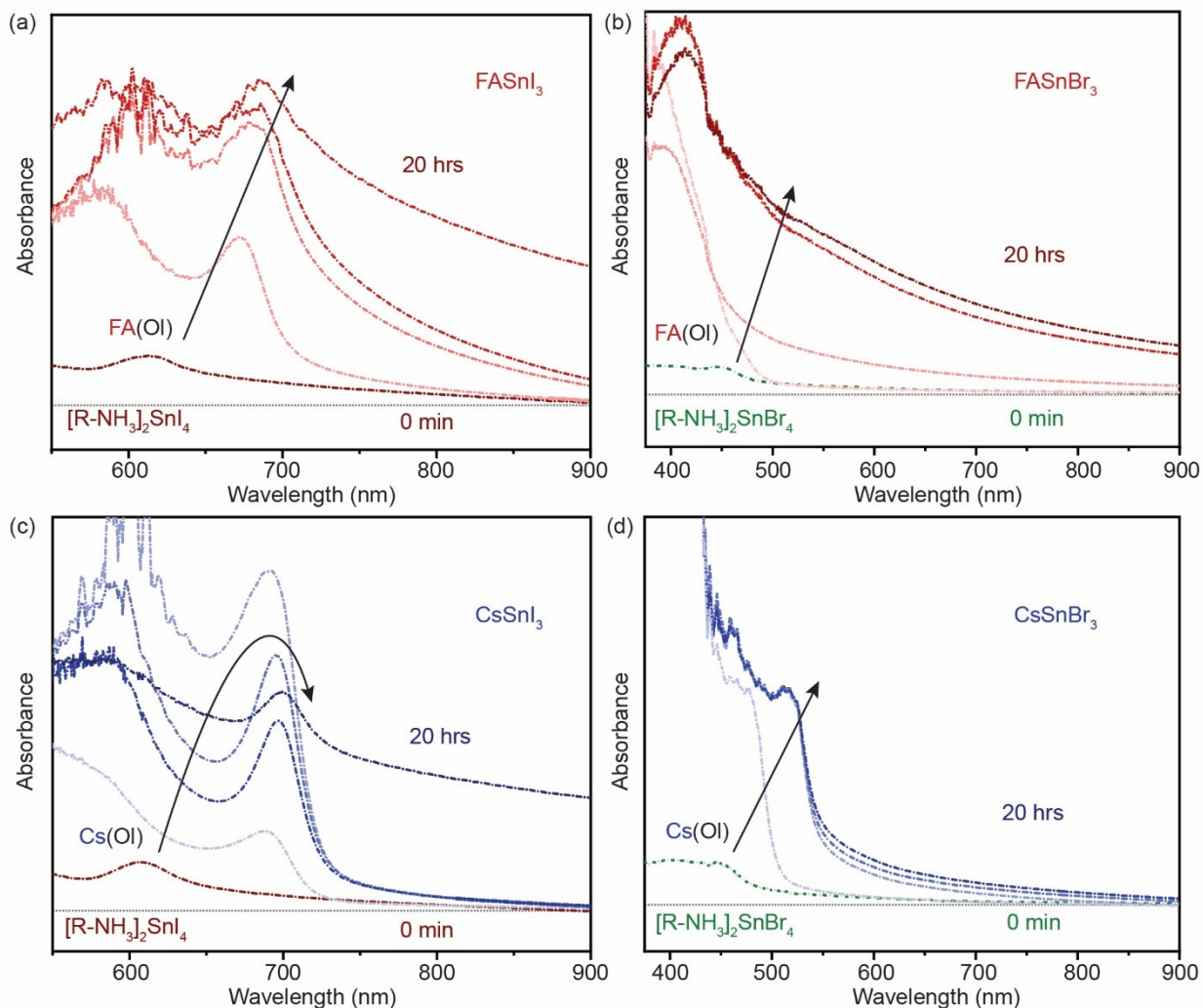


Figure S4. Extended time-dependence optical measurements (a) and (b) Insitu UV-Visible spectroscopy of the formation of 3D FASnI<sub>3</sub> and FASnBr<sub>3</sub> NCs with the addition of FA(OI) in 2D [R-NH<sub>3</sub>]<sub>2</sub>SnI<sub>4</sub> and [R-NH<sub>3</sub>]<sub>2</sub>SnBr<sub>4</sub> RP structures respectively over the time of 30 minutes. (c) and (d) Insitu UV-Visible spectroscopy of the formation of 3D CsSnI<sub>3</sub> and CsSnBr<sub>3</sub> NCs with the addition of Cs(OI) in 2D [R-NH<sub>3</sub>]<sub>2</sub>SnI<sub>4</sub> and [R-NH<sub>3</sub>]<sub>2</sub>SnBr<sub>4</sub> RP structures respectively over the time of 30 minutes.

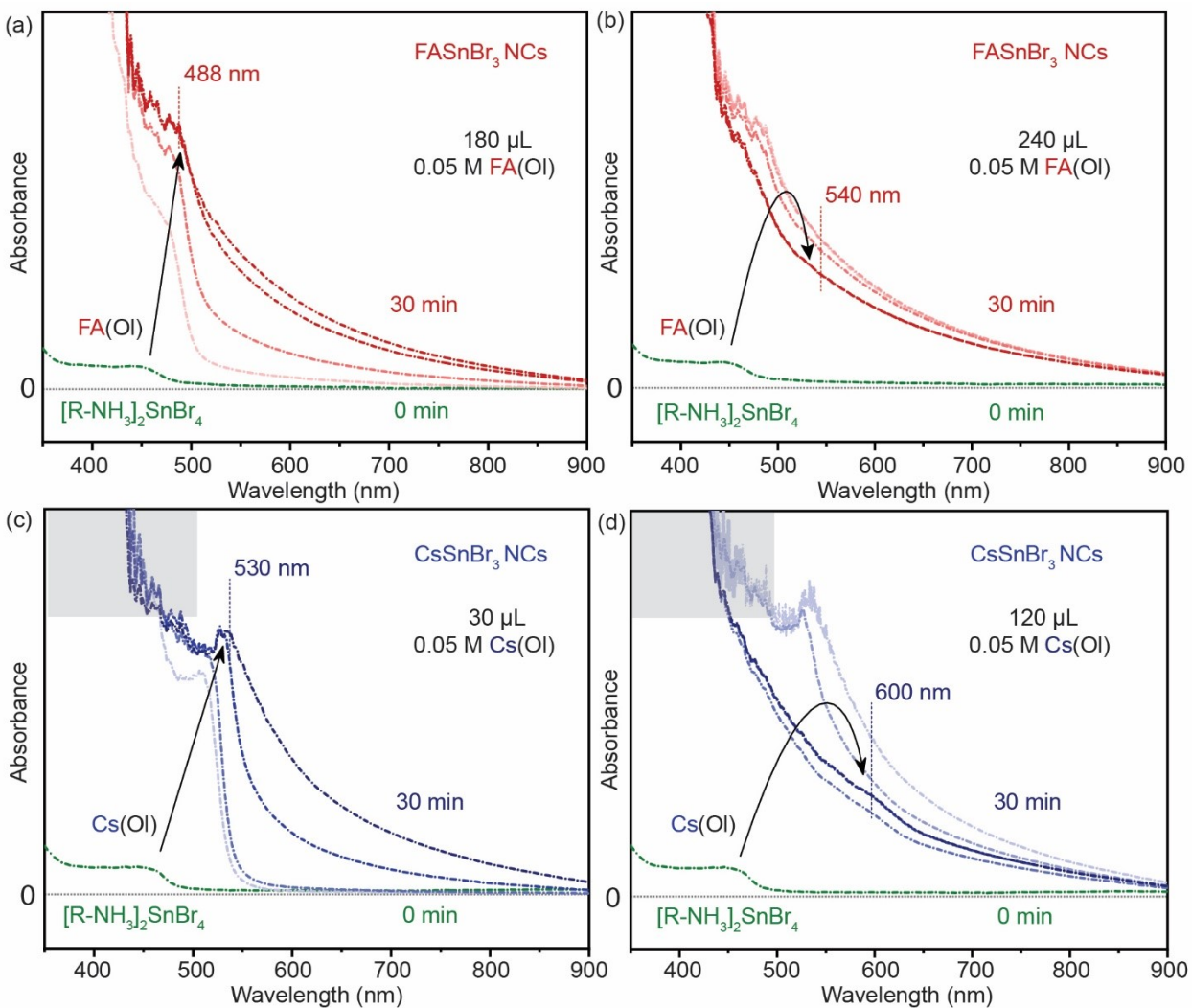
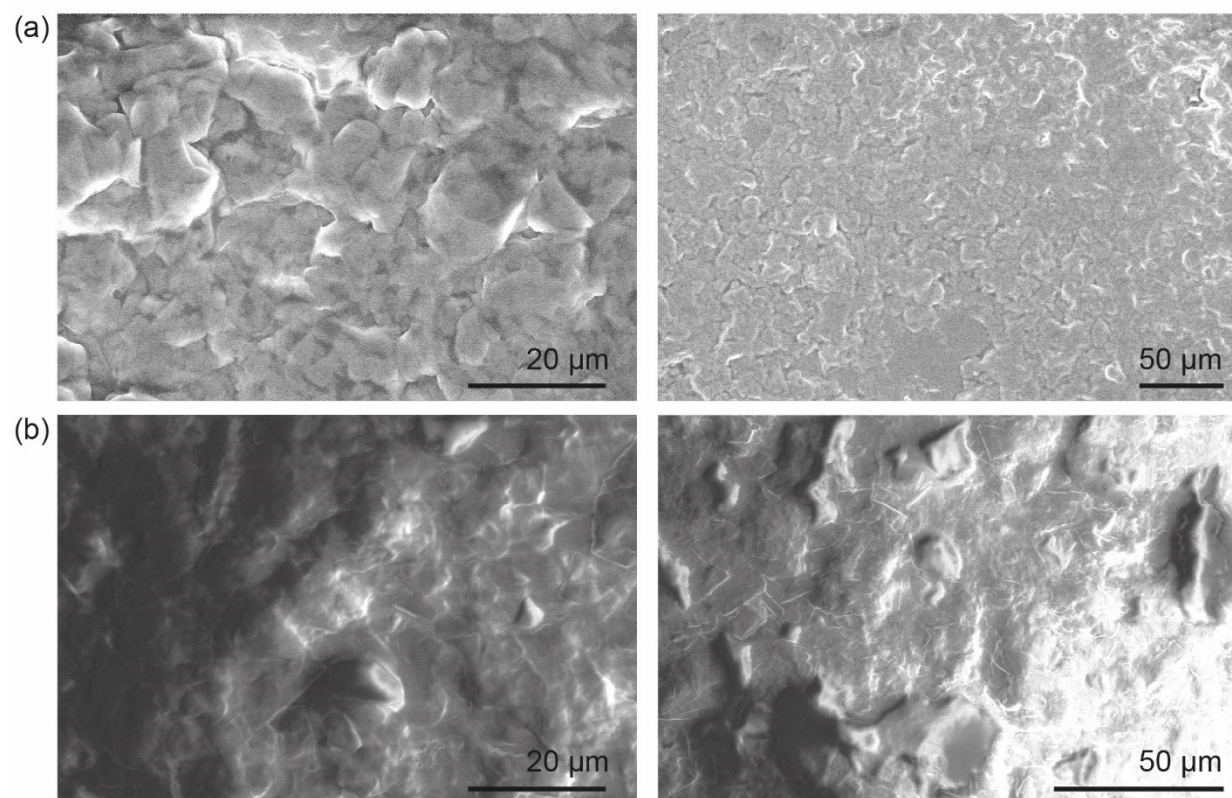


Figure S5. Concentration dependence (a) and (b) *In situ* UV-Visible spectroscopy of the formation of 3D FASnBr<sub>3</sub> (red) NCs with the addition of FA(OI) in 2D [R-NH<sub>3</sub>]<sub>2</sub>SnBr<sub>4</sub> RP structures over the time of 30 minutes. (c) and (d) *In situ* UV-Visible spectroscopy of the formation of 3D CsSnBr<sub>3</sub> (blue) NCs with the addition of Cs(OI) in 2D [R-NH<sub>3</sub>]<sub>2</sub>SnBr<sub>4</sub> RP structures over the time of 30 minutes.



*Figure S6. SEM images in the through the lens (TLD) mode. (a) Thin-film of 2D [R-NH<sub>3</sub>]<sub>2</sub>SnBr<sub>4</sub> RP nanostructures. (b) Thin-film of 2D [R-NH<sub>3</sub>]<sub>2</sub>SnI<sub>4</sub> RP nanostructures.*



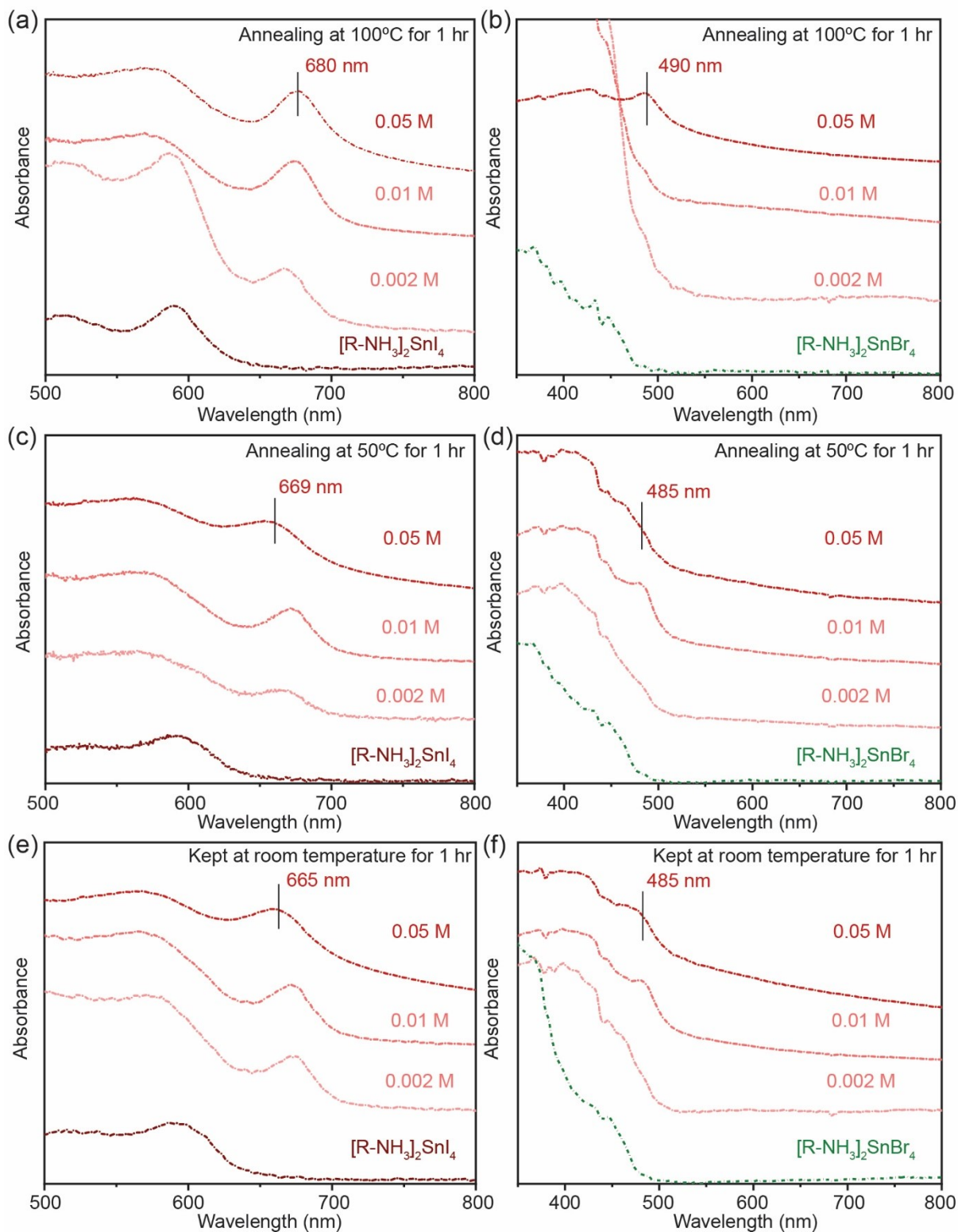


Figure S7. Annealing temperature dependence in Sn-halide perovskite thin-films with A cation addition at different concentrations. UV-Visible spectroscopy of the formation of 3D FASnI<sub>3</sub> and 3D FASnBr<sub>3</sub> nanostructures with the addition of FA(OI) on thin-film of 2D  $[R-NH_3]_2SnI_4$  RP nanostructures annealed at room temperature ((e) and (f)), 50°C ((c) and (d)) and 100°C ((a) and (b)) for an hour.

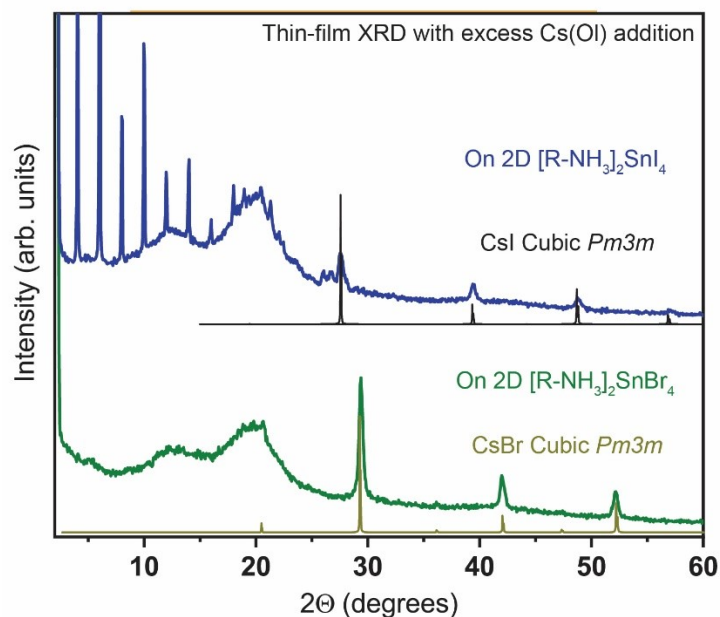


Figure S8. Powder X-ray diffraction pattern of the degraded thin-film with excess addition of Cs(OI) solution (30  $\mu$ L of 0.05 M solution) on 2D  $[R-NH_3]_2SnBr_4$  (green) and 2D  $[R-NH_3]_2SnI_4$  (blue). The XRD bulk references are plotted for CsI (cubic,  $Pm3m$ ) and CsBr (cubic,  $Pm3m$ ).<sup>3</sup>

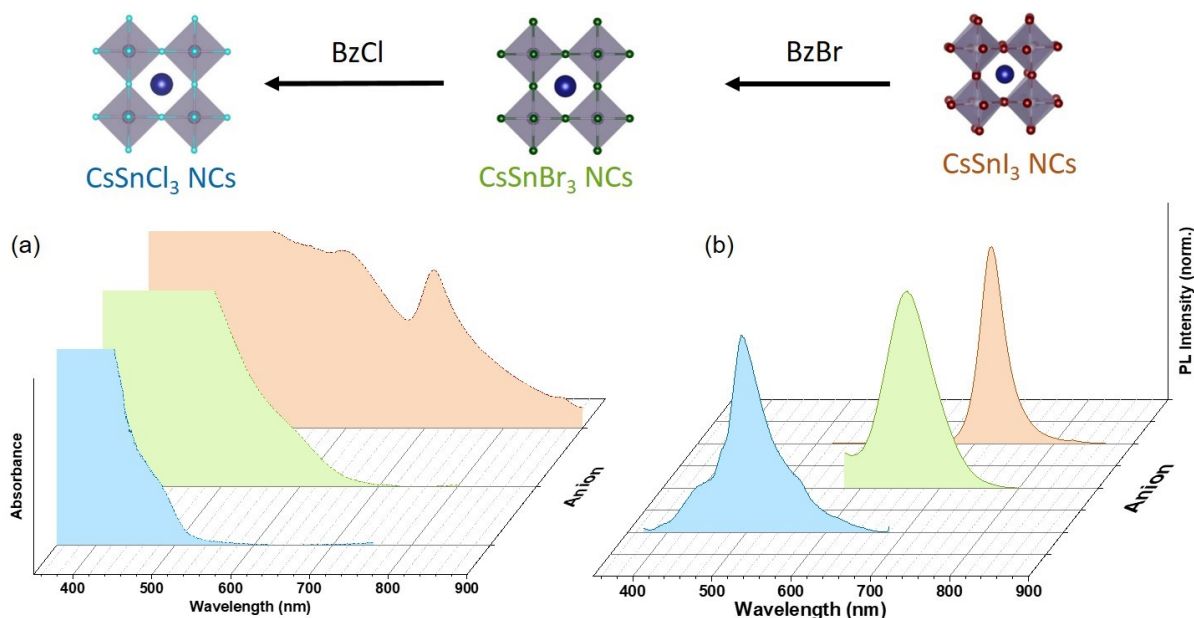


Figure S9. Anion exchange processes in solution of  $CsSnI_3$  NCs. (a) UV-Visible spectroscopy of 3D  $CsSnBr_3$  NCs formed via Br anion exchange of 3D  $CsSnI_3$  NCs performed at room temperature which further exchanged with Cl to form 3D  $CsSnCl_3$  NCs. (b) Photoluminescence spectroscopy of 3D  $CsSnBr_3$  NCs formed via Br anion exchange of 3D  $CsSnI_3$  NCs performed at room temperature which further exchanged with Cl to form 3D  $CsSnCl_3$  NCs.

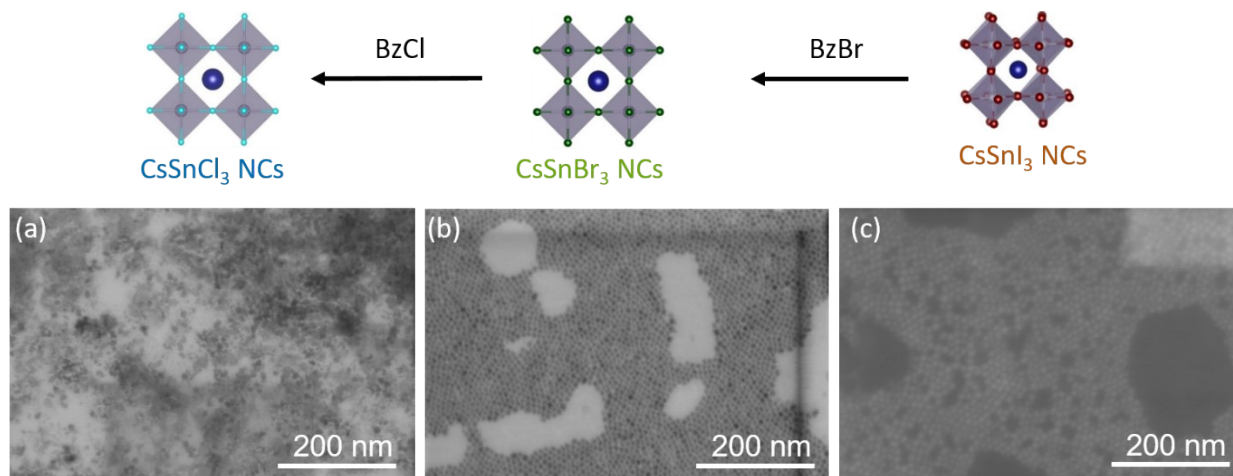


Figure S10. Anion exchange processes in solution of  $\text{CsSnI}_3$  NCs. (a) and (b) show the SEM micrographs of anion-exchanged 3D  $\text{CsSnBr}_3$  NCs formed via Br exchange of 3D  $\text{CsSnI}_3$  NCs and 3D  $\text{CsSnCl}_3$  NCs via a Cl exchange of 3D  $\text{CsSnBr}_3$  NCs formed earlier respectively. (c) SEM micrographs of  $\text{CsSnI}_3$  NCs before anion exchange.

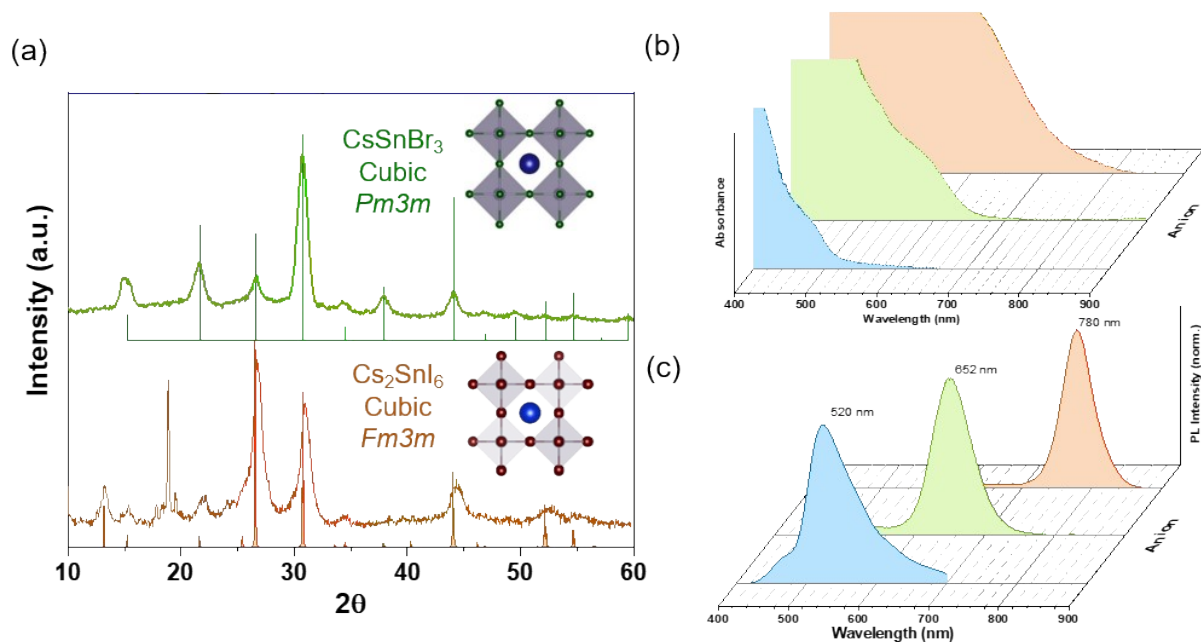


Figure S11. Anion exchange processes in solution of  $\text{CsSnBr}_3$  NCs. (a) Powder X-ray diffraction pattern of the Iodide exchanged  $\text{CsSnBr}_3$  NCs which yield  $\text{Cs}_2\text{SnI}_6$  NCs with excess  $\text{BzI}$  addition. (b) and (c) UV-Visible and PL spectroscopy anion exchanged sample of  $\text{CsSnCl}_3$  NCs (blue) and  $\text{Cs}_2\text{SnI}_6$  NCs (dark orange) with starting composition  $\text{CsSnBr}_3$  NCs for comparison. The XRD bulk references are plotted from  $\text{CsSnBr}_3$  (cubic,  $\text{Pm}3\text{m}$ )<sup>2</sup> and  $\text{Cs}_2\text{SnI}_6$  (cubic,  $\text{Fm}3\text{m}$ )<sup>4</sup>

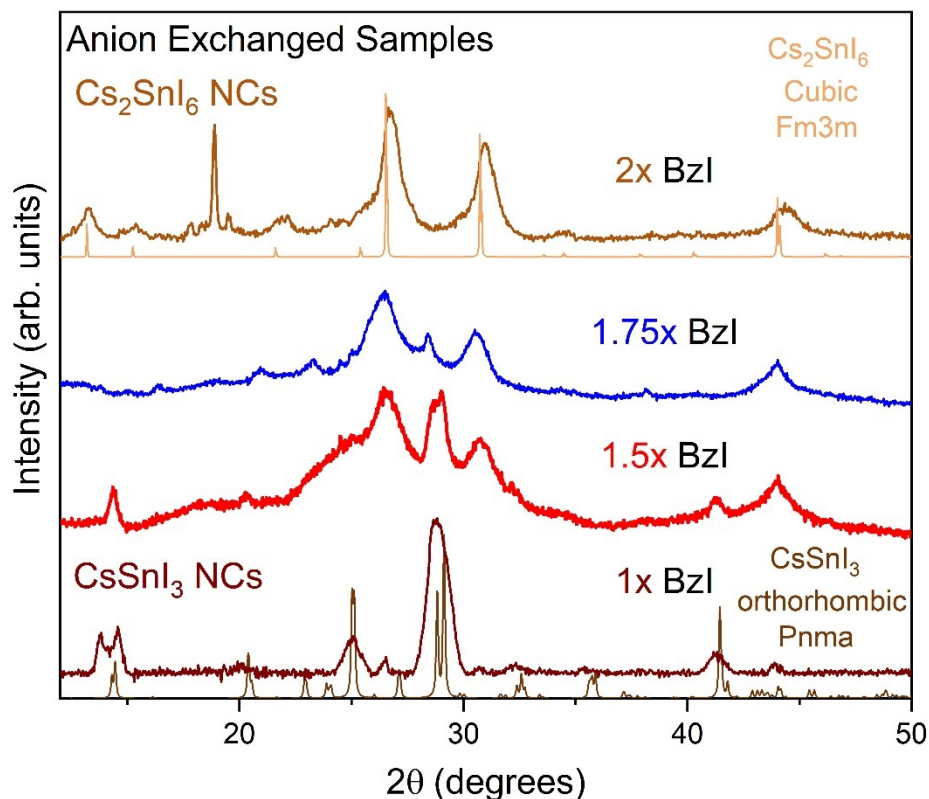


Figure S12. Evolution of powder X-ray diffraction pattern with increasing amount of BzI added for anion exchange. The XRD bulk references are plotted from  $\text{CsSnI}_3$  (orthorhombic,  $Pnma$ )<sup>5</sup> and  $\text{Cs}_2\text{SnI}_6$  (cubic,  $Fm3m$ )<sup>4</sup>

#### References:

1. M. Morana, J. Wiktor, M. Coduri, R. Chiara, C. Giacobbe, E. L. Bright, F. Ambrosio, F. De Angelis and L. Malavasi, *J. Phys. Chem. Lett.*, 2023, **14**, 2178-2186.
2. D. H. Fabini, G. Laurita, J. S. Bechtel, C. C. Stoumpos, H. A. Evans, A. G. Kontos, Y. S. Raptis, P. Falaras, A. Van der Ven, M. G. Kanatzidis and R. Seshadri, *J. Am. Chem. Soc.*, 2016, **138**, 11820-11832.
3. R. W. G. Wyckoff, *Crystal Structures - Volume 1*, Interscience Publishers New York, New York, 2nd ed edn., 1963.
4. C. C. Stoumpos, C. D. Malliakas and M. G. Kanatzidis, *Inorg. Chem.*, 2013, **52**, 9019-9038.
5. I. Chung, J.-H. Song, J. Im, J. Androulakis, C. D. Malliakas, H. Li, A. J. Freeman, J. T. Kenney and M. G. Kanatzidis, *J. Am. Chem. Soc.*, 2012, **134**, 8579-8587.